Performance Characterization of LCLS-II Superconducting Radiofrequency Cryomodules

Hieu Le[1] and Elvin Harms[2]

[1] *Dickinson College, Carlisle, PA 17013*
[2] *Fermilab, Batavia, IL 60540*

August 9, 2018

Abstract

The LCLS-II (Linac Coherent Light Source) is a 2nd generation X-ray free electron laser currently being constructed at SLAC. Fermilab is responsible for the design, construction and testing of seventeen 1.3 GHz and two 3.9 GHz cryomodules used in the LCLS-II. We developed tools in R to analyze the recorded testing data in a way that could not be done by Fermilab's ACNET system, and used them to investigate the performance of cryomodule F1.3-08 and F1.3-10.

1 Introduction

The LCLS-II (Linac Coherent Light Source) is a 2nd generation X-ray free electron laser upgrade to the current LCLS at SLAC National Accelerator Laboratory. LCLS-II is designed to produce 1 million X-ray pulses per second, compare to 120 pulses per second of the LCLS. LCLS-II is based on a 4 GeV superconducting electron linac and consists of thirty-five 1.3 GHz and two 3.9 GHz superconducting radiofrequency (SRF) cryomodules. Fermilab is responsible for designing these cryomodules, constructing and testing seventeen 1.3 GHz and both 3.9 GHz SRF cryomodules, each with eight 9-cells niobium SRF cavities [1].

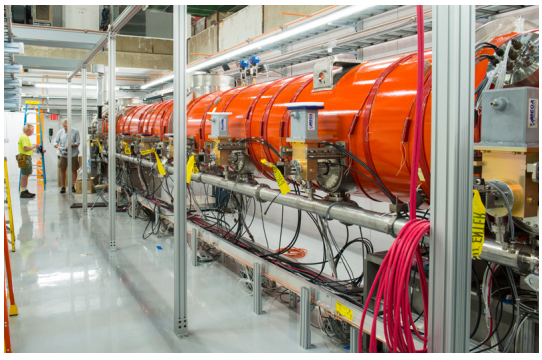

Figure 1: *LCLS-II cryomodule in the CMTS-1 test cave.*

Cryomodules built at Fermilab are tested in the Cryomodule Test Stand (CMTS-1) test cave at Fermilab's Cryomodule Test Facility (CMTF). The test stand is equipped with various data collecting equipment, in particular radiation detectors. The layout of these detectors in the test cave is shown in Fig. 2. 'Chipmunks', 'scarecrows' and 'FOXs' are local vernaculars for Fermilab-built radiation detectors [2], while TLM (Total Loss Monitor) is another type of detector that specializes in detecting beam loss over extensive regions in beam line enclosures [3]. The additional detectors - named DecaRad - were installed in the test cave just before the testing of cryomodule F1.3-10. All test data are collected and stored via Fermilab's ACNET (Accelerator Controls Network).

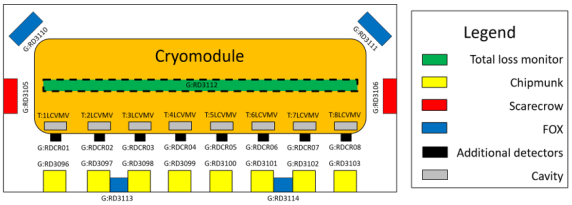

Figure 2: *Radiation detector layout within the test cave with ACNET device names. TLM is under the cryomodule, as expressed by the dashed lines.*

For the purpose of this paper, we will focus on the cryomodule testing process. In order to analyze testing data, we use R [4] - a programming language that specializes in statistical computing. R was chosen due to its extensive documentation, rate of usage at Fermilab and it being an interpreted language, thus easier to use and debug than compiled languages such as C++.

2 Testing and Purpose

2.1 Testing procedure

Before a cryomodule can be transported to SLAC for installation, it undergoes rigorous testing at Fermilab to ensure that the cryomodule meets stringent performance criteria. Primary criteria include individual cavity gradient of 16 MV/m, field emission onset $\geq$ 14 MV/m, average cavity $Q_0 \geq 2.7 \times 10^{10}$, and more [8]. Testing procedure can include the following processes (not exhaustive) [9]:

1. Mapping and setting Q_L
2. System calibration and calculating gradient
3. Performing power rise to evaluate peak gradient and field emission
4. Magnet testing
5. Measuring static heat load and higher order modes (HOM's)
6. Measuring dynamic heat load and intrinsic quality factor Q_0
7. Unit testing.

An important part of testing is monitoring for field electron emission during power rise. Field emission (FE) is one of the most important limiting factors in terms of cavity gradient. FE can interfere with cavity operation and lead to operational limitation due to radiation provided, and if intense enough can lead to thermal breakdown and quenching [5].

2.2 Devices

A goal of cryomodule testing is assessing FE status for each cavity, including onset, intensity, location and range of FE. This can be done by analyzing test cave radiation, dark current and cavity gradient data using tools that are described in the next section. We will mainly focus on data collected by the following devices for FE analysis, along with their names on ACNET servers

- Cavity gradient (T:1LCVMV - T:8LCVMV)
- Wall chipmunks (G:RD3096 - 3103)
- North/South scarecrows (G:RD3105 - 3106)
- Total loss monitor (G:RD3112)
- Feed/Endcap Faraday cups (T:8IDCFC, T:8IDCEC)
- DecaRad system (G:RDCR01 - 08)

2.3 Field emission

Electrons in metal are confined from escaping into vacuum by a potential well. In the presence of a high electric field, the potential barrier is lowered and electrons can tunnel out of the cavity wall at localized points, usually surface impurities. This field electron emission is then accelerated by the cavity, giving rise to a field emission current (dark current) which is governed by the Fowler-Nordheim equation [5]

$$I \propto (\beta_{FN} E)^{2.5} \exp\left(\frac{-B_{FN}\phi^{3/2}}{\beta_{FN} E}\right) \qquad (1)$$

where E is the cavity gradient in MV/m, ϕ is the niobium workfunction, β_{FN} is the field enhancement factor, and $B_{FN} = 6.83 \times 10^3$.

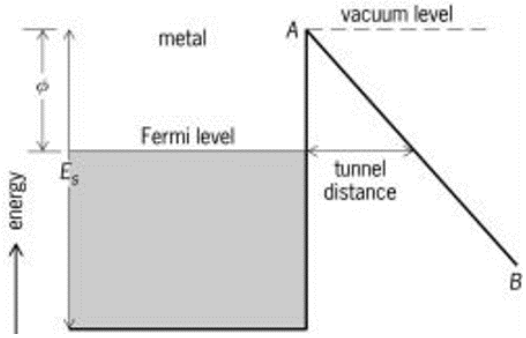

Figure 3: *Fowler-Nordheim tunneling governing field emission. Vacuum potential barrier is lowered by the applied electric field.*

Since field emission occurs at localized sites, emitter locations can be determined via bremsstrahlung radiation, which is X-ray radiation emitted when electrons are deflected by the cavity wall and is approximately [6]

$$\dot{N} \propto (\beta_{FN} E)^{2.5} E^5 \exp\left(\frac{-B_{FN} v(y) \phi^{3/2}}{\beta_{FN} E}\right). \qquad (2)$$

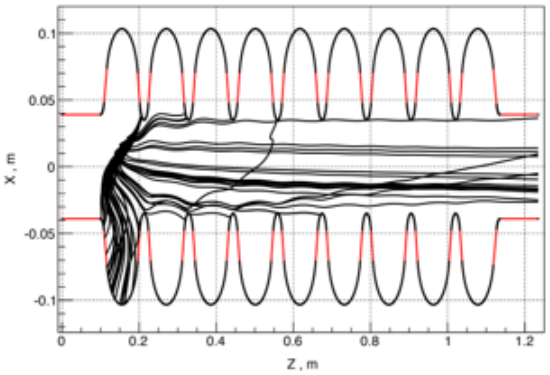

Figure 4: *Movement of FE electrons from a site in the cavity. Electrons that hit the cavity wall give bremsstrahlung, while electrons that go down the cavity give dark current. [A. Sukhanov]*

Field emission can sometimes be reduced or eliminated via a processing event. Under sufficiently high cavity gradient, the emitter has a chance to be destroyed, leaving behind a starburst-shaped crater region and molten particles. Sometimes the available continuous wave (cw) power is insufficient to raise the gradient high enough to trigger a processing event; in which case we resort to high power pulsed processing (HPP). HPP allows the cavity to reach higher gradient than cw, hopefully enough to process away the emitters, while minimizing power dissipation into liquid helium by delivering very short and high power pulses [7].

3 Analysis Tools

3.1 Data wrangling

Data wrangling is often the first step in data analysis, which includes taking raw data and transforming it into a more convenient format. Cryomodule test data on ACNET can be exported to an Excel file (technically tab-separated values) in the format as shown in Fig. 5. This format includes logged values for each device as well as timestamp for each data point. ACNET can export up to 8 devices per file. Often, we would like to explore the relationship between more than 8 devices, or between different device types with different data logging rates. Using R and various R packages, we developed a data wrangling process for cryomodule testing data (note: packages or specific functions involved will from now on be specified in square brackets)

1. Import files to R environment as a list of data frame objects [rio]
2. Split data frames up by Time/Device pairs
3. Convert timestamps from each data frame from strings to date-time objects
4. Join Time/Device pairs, preserving data from all pairs [data.table]

After this process, we now have a list of data frames; each corresponds to an imported file. In a data frame, all excess Time columns are eliminated while data from all devices are preserved regardless of logging rate as seen in Fig. 6. Although this process takes care of all devices regardless of logging rate, it is highly recommended that the user limits to one type of device per file, as many devices with different logging rates can unnecessarily enlarge the data frame since the process preserves all timestamps introduced.

	Time	G:RD3096	Time	G:RD3097	Time	G:RD3098	Time	G:RD3099	Time
1	Mon Jul 30 11:01:01.444	0.15	Mon Jul 30 11:01:01.444	0.15	Mon Jul 30 11:01:01.444	0.15	Mon Jul 30 11:01:01.444	0.15	Mon Jul 30 1
2	Mon Jul 30 11:02:01.444	0.00	Mon Jul 30 11:02:01.444	0.15	Mon Jul 30 11:02:01.444	0.15	Mon Jul 30 11:02:01.444	0.15	Mon Jul 30 1
3	Mon Jul 30 11:03:01.427	0.15	Mon Jul 30 11:03:01.427	0.15	Mon Jul 30 11:03:01.427	0.15	Mon Jul 30 11:03:01.427	0.15	Mon Jul 30 1
4	Mon Jul 30 11:04:01.460	0.15	Mon Jul 30 11:04:01.460	0.15	Mon Jul 30 11:04:01.460	0.00	Mon Jul 30 11:04:01.460	0.15	Mon Jul 30 1
5	Mon Jul 30 11:05:01.477	0.15	Mon Jul 30 11:05:01.477	0.00	Mon Jul 30 11:05:01.477	0.15	Mon Jul 30 11:05:01.477	0.15	Mon Jul 30 1
6	Mon Jul 30 11:06:01.510	0.15	Mon Jul 30 11:06:01.510	0.15	Mon Jul 30 11:06:01.510	0.15	Mon Jul 30 11:06:01.510	0.15	Mon Jul 30 1
7	Mon Jul 30 11:07:01.527	0.15	Mon Jul 30 11:07:01.527	0.30	Mon Jul 30 11:07:01.527	0.15	Mon Jul 30 11:07:01.527	0.00	Mon Jul 30 1
8	Mon Jul 30 11:08:01.544	0.15	Mon Jul 30 11:08:01.544	0.15	Mon Jul 30 11:08:01.544	0.15	Mon Jul 30 11:08:01.544	0.15	Mon Jul 30 1
9	Mon Jul 30 11:09:01.527	0.15	Mon Jul 30 11:09:01.527	0.15	Mon Jul 30 11:09:01.527	0.15	Mon Jul 30 11:09:01.527	0.15	Mon Jul 30 1
10	Mon Jul 30 11:10:01.510	0.30	Mon Jul 30 11:10:01.510	0.15	Mon Jul 30 11:10:01.510	0.15	Mon Jul 30 11:10:01.510	0.15	Mon Jul 30 1
11	Mon Jul 30 11:11:01.527	0.15	Mon Jul 30 11:11:01.527	0.15	Mon Jul 30 11:11:01.527	0.15	Mon Jul 30 11:11:01.527	0.15	Mon Jul 30 1
12	Mon Jul 30 11:12:01.510	0.15	Mon Jul 30 11:12:01.510	0.30	Mon Jul 30 11:12:01.510	0.30	Mon Jul 30 11:12:01.510	0.15	Mon Jul 30 1
13	Mon Jul 30 11:13:01.510	0.30	Mon Jul 30 11:13:01.510	0.15	Mon Jul 30 11:13:01.510	0.15	Mon Jul 30 11:13:01.510	0.30	Mon Jul 30 1
14	Mon Jul 30 11:14:01.510	0.15	Mon Jul 30 11:14:01.510	0.30	Mon Jul 30 11:14:01.510	0.15	Mon Jul 30 11:14:01.510	0.15	Mon Jul 30 1
15	Mon Jul 30 11:15:01.510	0.30	Mon Jul 30 11:15:01.510	0.15	Mon Jul 30 11:15:01.510	0.30	Mon Jul 30 11:15:01.510	0.15	Mon Jul 30 1
16	Mon Jul 30 11:16:01.510	0.30	Mon Jul 30 11:16:01.510	0.45	Mon Jul 30 11:16:01.510	0.15	Mon Jul 30 11:16:01.510	0.30	Mon Jul 30 1
17	Mon Jul 30 11:17:01.510	0.45	Mon Jul 30 11:17:01.510	0.30	Mon Jul 30 11:17:01.510	0.30	Mon Jul 30 11:17:01.510	0.30	Mon Jul 30 1
18	Mon Jul 30 11:18:01.527	0.45	Mon Jul 30 11:18:01.527	0.45	Mon Jul 30 11:18:01.527	0.45	Mon Jul 30 11:18:01.527	0.30	Mon Jul 30 1
19	Mon Jul 30 11:19:01.510	0.45	Mon Jul 30 11:19:01.510	0.45	Mon Jul 30 11:19:01.510	0.30	Mon Jul 30 11:19:01.510	0.30	Mon Jul 30 1

Figure 5: *Original imported data format. Each device is accompanied by a timestamp column, which is inconvenient.*

	Time	G:RD3096	G:RD3097	G:RD3098	G:RD3099	G:RD3100	G:RD3101	G:RD3102	G:RD3103
1	2018-07-30 11:01:01.444	0.15	0.15	0.15	0.15	0.15	0.00	0.15	0.15
2	2018-07-30 11:02:01.444	0.00	0.15	0.15	0.15	0.15	0.15	0.15	0.00
3	2018-07-30 11:03:01.427	0.15	0.15	0.15	0.15	0.15	0.15	0.15	0.15
4	2018-07-30 11:04:01.460	0.15	0.15	0.00	0.15	0.15	0.15	0.15	0.15
5	2018-07-30 11:05:01.476	0.15	0.00	0.15	0.15	0.15	0.00	0.00	0.15
6	2018-07-30 11:06:01.509	0.15	0.15	0.15	0.15	0.15	0.15	0.15	0.15
7	2018-07-30 11:07:01.526	0.15	0.30	0.15	0.00	0.15	0.15	0.15	0.00
8	2018-07-30 11:08:01.543	0.15	0.15	0.15	0.15	0.15	0.00	0.15	0.15
9	2018-07-30 11:09:01.526	0.15	0.15	0.15	0.15	0.15	0.15	0.15	0.15
10	2018-07-30 11:10:01.509	0.30	0.15	0.15	0.15	0.15	0.15	0.15	0.15
11	2018-07-30 11:11:01.526	0.15	0.15	0.15	0.15	0.15	0.15	0.00	0.00
12	2018-07-30 11:12:01.509	0.15	0.30	0.30	0.15	0.15	0.00	0.15	0.15
13	2018-07-30 11:13:01.509	0.30	0.15	0.15	0.30	0.30	0.15	0.15	0.15
14	2018-07-30 11:14:01.509	0.15	0.30	0.15	0.15	0.15	0.15	0.15	0.15
15	2018-07-30 11:15:01.509	0.30	0.15	0.30	0.15	0.15	0.15	0.15	0.15
16	2018-07-30 11:16:01.509	0.30	0.45	0.15	0.30	0.15	0.15	0.15	0.15
17	2018-07-30 11:17:01.509	0.45	0.30	0.30	0.30	0.30	0.15	0.15	0.15
18	2018-07-30 11:18:01.526	0.45	0.45	0.45	0.30	0.30	0.15	0.15	0.15
19	2018-07-30 11:19:01.509	0.45	0.45	0.30	0.30	0.15	0.15	0.15	0.15
20	2018-07-30 11:20:01.526	0.45	0.60	0.45	0.30	0.30	0.30	0.15	0.15
21	2018-07-30 11:21:01.543	0.60	0.45	0.45	0.30	0.30	0.15	0.15	0.15

Figure 6: *Cleaned data format. Excess timestamp columns are removed, and the 'Time' column is now a date-time object.*

Next, we would like to join all data frames in the list. To do this, the user starts by specifying a list of devices of interest. This is not required for small data sets, but for big data sets (approximately 100 Mb and above) it is recommended to not select all devices to not slow down the process. The script then go through all data frames in the list and pick out devices that match the specified names, then join them to the data frame with the largest number of data points by nearest timestamp [data.table], so as not to miss any data point while staying at a manageable size. The result is a data frame complete with timestamp as date-time objects and all devices of interest with all data preserved. This is the backbone of all other tools developed in the following sections.

3.2 Data visualization

A crucial part of exploratory data analysis is data visualization. We would like to be able to explore time series plots of devices as well as their relationships with each other in an efficient way, both for reactive troubleshooting and logging data travelers for each cryomodule. Thus we developed a web application [shiny] that can be run both on the web for remote access and offline which takes in Excel files exported from ACNET and outputs an interactive, feature-rich plot [plotly, ggplot2].

The app incorporates previous data wrangling tool to process the data. Afterwards, the user can specify a variety of plot parameters, such as independent and dependent variables, time frames, and plot and axis labels. It is important that the user specify the time frames for large data sets, as plotting can take a long time without filtering. The app supports plots of one versus multiple devices and time series plots. The plot output is highly interactive and comes with a variety of features, including but not limited to hiding/showing data for certain devices, returning values of points upon hovering, zooming in/out, exporting, etc.

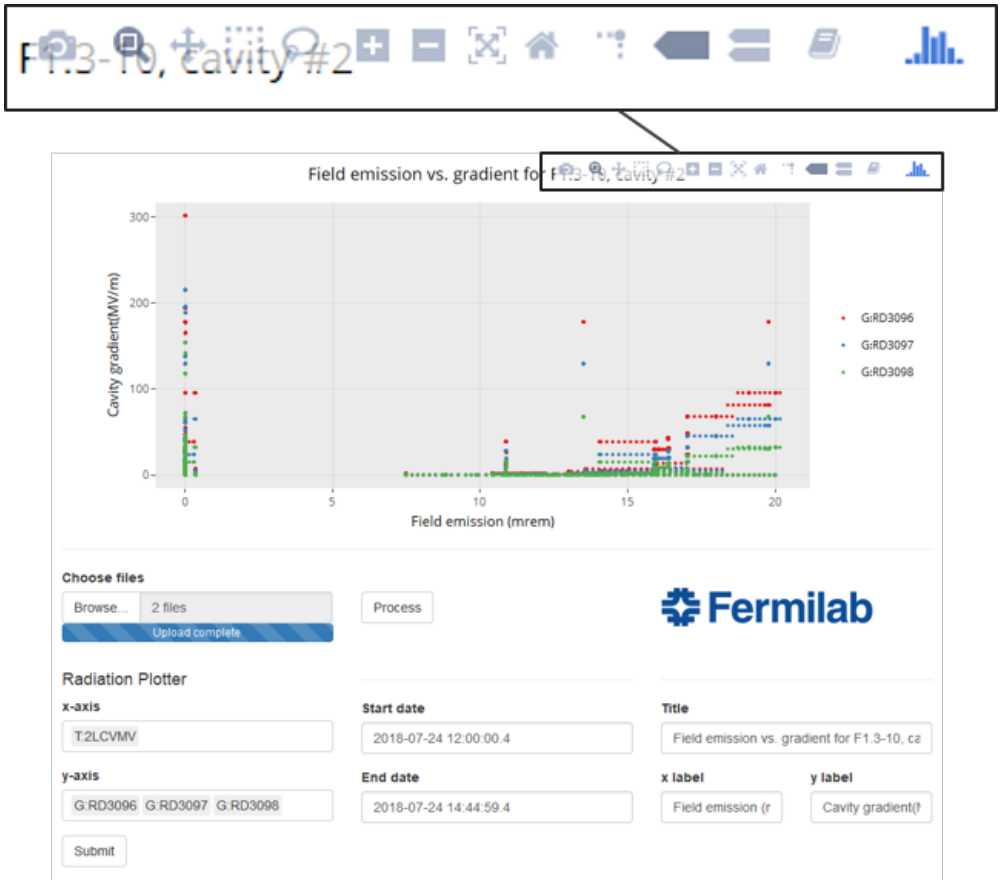

Figure 7: *Layout of the web application. Some interactive features can be seen from the toolbar on the top right corner of the figure.*

For further investigation with more complicated and detailed plots, manual plotting is required [ggplot2]. A brief guide for this process is in the documentation for the project. Future work can include incorporating this into the web app.

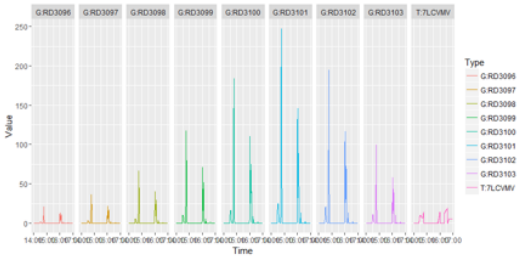

Figure 8: *An example of a type of graph that is currently only able to be plotted manually.*

3.3 Model fitting

In order to have a complete characterization of a cryomodule, we would like to investigate the onset of FE for each cavity. Since chipmunk data is logged every minute (1/60 Hz), it is possible for the true FE onset to be lower than the observed onset level. We looked for a way to evaluate the true onset level using a variety of model fits.

3.3.1 Field emission radiation

For FE radiation data, we tested a log-linear transform model [lm] of the form $\ln y = Ax + B$, or $y = Ce^{Ax}$. This model is fitted with the condition that the background level is close to zero, as the log-linear transform model has no y-intercept. One challenge with this model is the fact that FE does not show up until a certain gradient level. Below that level, radiation count stays at background, which when fitted with a logarithmic model does not return a model with great accuracy, due to the constant "tail" of the data distribution. We circumvented this issue by manually specifying thresholds at which the model will be fitted, under the assumption that small variations in the threshold around the true onset point results in small variations in the model and consequently, small variations in predicted true onset. We tested the model and found good agreement between the model and the actual data set. We then predicted the actual onset by the point at which the model deviates significantly from background; in this case when the model crosses a

specified level.

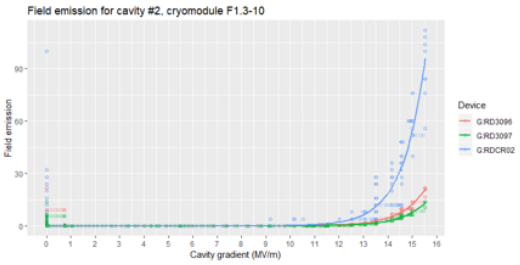

Figure 9: *Log-linear transform model* $\ln y = Ax + B$ *for FE radiation. Note the difference between the models near the onset point. The blue line repsresents DecaRad #2, the rest are chipmunks.*

As the chipmunks are located some distance away (4 meters) from the cavities, usually multiple chipmunks will pick up FE radiation activity from a cavity at different magnitudes. Furthermore immediately before F1.3-10 testing, CMTS-1 installed the DecaRad system located directly in front of the cavities which has a different reading scale than that of the chipmunks. This results in different predicted onset levels across devices due to the logarithmic model fitting and our method of predicting onset. We would like to cross-check FE onset across different devices, and thus we employed quantile normalization method. This method transforms data to have a common distribution of intensities, under the assumption that the data sets have similar distributions (in this case, FE radiation distribution). Normalization is achieved by forcing the observed distributions to be the same using the average distribution - obtained by taking the average of each quantile across samples - as reference [10]. We see that after applying quantile normalization, all 3 devices have approximately the same predicted onset, therefore the DecaRad system and chipmunk show the same level of onset for a cavity.

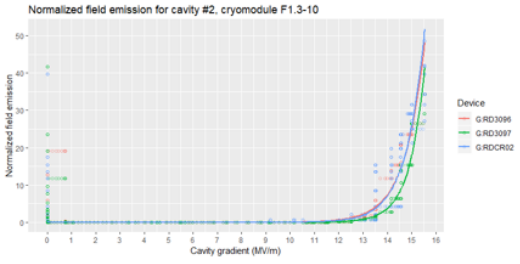

Figure 10: *Normalized log-linear transform model.*

3.3.2 Dark current

For dark current data, we tested a similar model to that from the previous section. We ran into an immediate challenge: the dark current data includes data points with negative values. We resolved this by subtracting the smallest value in the whole data set from the data set. However, the background level for dark current is now no longer close to zero, thus the assumption for the log-linear transformed model fails.

Since dark current is directly related to the Fowler-Nordheim (FN) equation, we decided to use nonlinear least squares [nls] to fit the FN model of the form $y = Ax^{2.5}\exp(-B/x) + C$ derived from Eq. 1 to the data set. The default algorithm for R's [nls] function is Gauss-Newton algorithm (also called multivariate Newton-Raphson), which is an iterative method that requires an initial guess [11, 12]. For the algorithm to converge, the initial estimates must be "close enough".

A way to estimate these parameters is by applying a linear regression to the series expansion of the FN model. This has the form $C + Ax^{2.5}\exp(-B/x) = C + Ax^{2.5}\left(1 - \frac{B}{x} + \frac{B^2}{2!x^2} - \frac{B^3}{3!x^3} + \frac{B^4}{4!x^4} + \mathcal{O}\left(\frac{1}{x^5}\right)\right)$. This method works most of the time for dark current data. We also found a certain set of initial values $A = 0.028$, $B = 30$, $C = 0.5$ that has so far performed very well for dark current data. In order to fit the model to the data set, we subtract the smallest value, fit the model then shift everything back to its original values. We see from Fig. 11 that the model fits the data well.

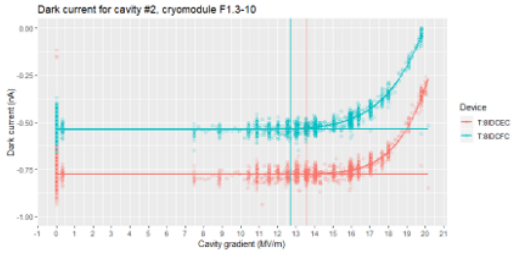

Figure 11: *Fowler-Nordheim model* $Ax^{2.5}e^{-\frac{B}{x}} + C$ *for dark current. Horizontal line is average background, while vertical line is predicted FE onset.*

The onset is calculated by first finding the average background level, subtract that from the FN fitted model, then finding the root of that equation using Newton-Raphson method with the function uniroot. This method requires the function evaluated at the start and end of the interval of interest to bracket the root (i.e. have different signs).

3.4 Challenges and future works

We encountered a fair number of challenges during the development process. One of the most troublesome ones was the inclusion of a colon in all ACNET devices name. Colons are reserved in R, thus it cannot be used normally as a character, although it can be used in character strings. One way to overcome this is to wrap all expressions including ACNET names in `eval(parse(text`

`= paste([concatenate strings here], sep = '')))`, however this is rather clunky and can be unsightly. Suggestion for future work can include removing all colons from ACNET device names when importing files, thus simplifying the process.

Another issue is that the online-hosted web application does not accept huge data files (approx. 150 Mb) while there is no such issue with the offline R script itself. There is no definite clue as to why this happens.

Additionally, as mentioned above we need a robust way of determining initial conditions for the [nls] function. One suggestion on how to do this is to map out the RMS values for the FN model with different coefficients as a function of the true values, and find the minimum of that function using gradient descent or other methods. Another suggestion would be to find out the actual physical parameters of niobium cavities, and finding the initial values using the FN equation (although the theoretical values might be different from real life ones). One can also look into using another method altogether, such as spline fitting, generalized linear model or linear regression of series expansion. Once a reliable method has been found, we would also like to apply it to fit Eq. 2 to the FE radiation data.

We would also like to have a more reliable way of finding FE onset. Currently the method of finding FE onset based on FE radiation depends on the assumption that perturbations to the model does not vary the onset too much, and the choices of thresholds can be rather arbitrary. Furthermore, sometimes the average background line and the fitted FN model line does not cross, which means the root finding algorithm fails; thus it needs more refinement.

Finally, we would like to have a complete calibration system between chipmunks, scarecrows, TLM and DecaRads. This will help in troubleshooting, and might give rise to some more interesting insights.

4 Results

We tested our developed data wrangling and visualization tools extensively with certain cryomodules, and found that they have been robust and effective in terms of data preprocessing.

We analyzed FE data for cryomodule F1.3-09 tested in March 2018 for cavity #5 and #6 to test the fitting models. There we predicted pre-HPP emission onset to be at 13 MV/m and 13.4 MV/m respectively. This agrees well with empirically determined data, thus showing that the fitted model works decently. We also applied the fitting tools to test data for cryomodule F1.3-08 in June and F1.3-10 in July, which is summarized in the table below.

Cryomodule & cavity	Predicted (MV/m)	Before HPP (MV/m)	Error (%)
F1.3-09 #5	13	15	13.3
F1.3-09 #6	13.4	14	4.29
F1.3-08 #7	6	7	14.29
F1.3-10 #2	13.1	12.5	4.8
F1.3-10 #5	12.8	15	14.7

Note that a smaller value with a high percentage of error is not necessarily bad, as onset can happen before data is logged into the system. From this results, we see that the fitted model works relatively well with the data but could benefit from more refinement.

5 Conclusion

We developed tools in R to process and analyze cryomodule testing data. With these tools, ACNET data (not limited to just cryomodule testing data) can now be processed in a way that allows for manipulation for many purposes. We can also visualize field emission data, which can help with reactive troubleshooting and logging data travelers for cryomodules. Furthermore, these developed tools can be applied to analyze data outside of cryomodule testing. Future improvements can include streamlining and optimizing, implementing extra tools into the developed web application, and more as outlined in Section 3.4.

6 Acknowledgement

This document was prepared by Hieu Le using the resources of the Fermi National Accelerator Laboratory (Fermilab), a U.S. Department of Energy, Office of Science, HEP User Facility. Fermilab is managed by Fermi Research Alliance, LLC (FRA), acting under Contract No. DE-AC02-07CH11359.

7 References

[1] Arkan, T. et al. (2015). *LCLS-II 1.3 GHz Design Integration for Assembly and Cryomodule Assembly Facility Readiness at Fermilab.* Proc. 17th Int. Conf. on RF Superconductivity (SRF2015), Whistler, BC, Canada

[2] Fermilab (2017). *FRCM Chapter 5: Radiological Health Support Operations.*

[3] Zhang, Y., Harms, E. (2014). *Evaluation of Total Loss Monitor for Cryomodule Radiation Measurement.*

[4] *The R Project for Statistical Computing.* (n.d.). Retrieved from https://www.r-project.org/

[5] Padamsee, H. S. (2009). *Rf Superconductivity: Science, Technology and Applications*. Weinheim: John Wiley & Sons.

[6] Schwettman, H. A., Turneaure, J. P. & Waites, R. F. (1974). *Evidence for surface-state-enhanced field emission in rf superconducting cavities*. Journal of Applied Physics 45, 914

[7] Padamsee, H., Knobloch, J., & Hays, T. (2008). *RF superconductivity for accelerators*. Weinheim: Wiley-VCH.

[8] Harms, E. et al. (2016). *Commissioning and First Results from the Fermilab Cryomodule Test Stand*. Proc. LINAC2016, East Lansing, MI, USA

[9] Harms, E. et al. (2015). *High Gradient Performance in Fermilab ILC Cryomodule*. Proc. 17th Int. Conf. on RF Superconductivity (SRF2015), Whistler, BC, Canada

[10] Hicks, S., Irizarry, R. (2015). *Quantro: A data-driven approach to guide the choice of an appropriate normalization method.*. Genome Biology, 16(1), 117

[11] Chapra, S. C. (2012). *Applied numerical methods with MATLAB for engineers and scientists*. New York: McGraw-Hill.

[12] *R: Nonlinear Least Squares*. (n.d.). Retrieved from https://stat.ethz.ch/R-manual/R-devel/library/stats/html/nls.html

[13] Wickham, H., & Grolemund, G. (2017). *R for data science: Import, tidy, transform, visualize and model data*. Sebastopol: O'Reilly.